Effects of helicity on dissipation in homogeneous box turbulence

Effects of helicity on dissipation in homogeneous box turbulence*

Moritz Linkmann†,

Fachbereich Physik, Philipps-Universität Marburg, Renthof 6, 35032 Marburg, Germany

(Received 20 April 2018; revised 18 July 2018; accepted 27 August 2018)

The dimensionless dissipation coefficient $\beta = \varepsilon L/U^3$, where ε is the dissipation rate, U the root-mean-square velocity and L the characteristic scale of the largest flow structures, is an important characteristic of statistically stationary homogeneous turbulence. In studies of β, the external force is typically isotropic and large scale, and its helicity H_f either zero or not measured. Here, we study the dependence of β on H_f and find that it decreases β by up to 10% for both isotropic forces and shear flows. The numerical finding is supported by static and dynamical upper bound theory. Both show a relative reduction similar to the numerical results. That is, the qualitative and quantitative dependence of β on the helicity of the force is well captured by upper bound theory. Consequences for the value of the Kolmogorov constant and theoretical aspects of turbulence control and modelling are discussed in connection with the properties of the external force. In particular, the eddy viscosity in large eddy-simulations of homogeneous turbulence should be decreased by at least 10% in the case of strongly helical forcing.

Key words: homogeneous turbulence, mathematical foundations, turbulence theory

1. Introduction

The Richardson-Kolmogorov cascade picture of fully developed turbulence relies on the assumption that the dissipation rate of turbulent kinetic energy remains finite in the limit of vanishing viscosity, i.e. on the dissipative anomaly (Frisch 1995; Eyink 2003). The behaviour of the mean dissipation rate ε as a function of viscosity is mostly studied in nondimensional terms through the Reynolds-number dependence of the dimensionless dissipation factor $\beta = \varepsilon L/U^3$ (Batchelor 1953), where U denotes the root-mean-square velocity and L the size of the largest eddies in the flow. The dimensionless dissipation rate is not only of interest in turbulence theory, as it enters adjustable coefficients in turbulence models such as the eddy viscosity in the k-ε model (Tannehill *et al.* 1997; Goto & Vassilicos 2009). The Smagorinsky constant in large-eddy simulations (LES) also depends on β. Since its introduction, the question remains as to whether the infinite-Reynolds-number asymptote of β is a universal quantity, i.e. whether it depends on the forces generating the turbulence and on the boundary conditions (Goto & Vassilicos 2009; Bos *et al.* 2007). Since β is related to the Kolmogorov constant C_K (Lumley 1992), the question of universality concerning β extends to the Kolmogorov constant. The latter has been an open question since the inference by Landau against universality of constants like C_K (Landau & Lifshitz 1959; Frisch 1995). In particular, it is very difficult to disprove universality for forces acting at one single characteristic scale, as is the case for turbulence

† Email address for correspondence: moritz.linkmann@physik.uni-marburg.de

generated by a uniform grid in e.g. a wind tunnel (Frisch 1995). The present paper examines the universality of β and C_K with respect to external forces which differ in their topological properties, namely their respective helicities, while acting at the same single characteristic length scale.

The value of β has been measured in experiments (Sreenivasan 1984, 1998; Burattini *et al.* 2005) as well as in direct numerical simulations (DNSs) (Wang *et al.* 1996; Kaneda *et al.* 2003; Gotoh *et al.* 2002; Donzis *et al.* 2005; Bos *et al.* 2007; Goto & Vassilicos 2009; Yeung *et al.* 2012; McComb *et al.* 2015; Yeung *et al.* 2015; Ishihara *et al.* 2016). Although the experiments differed in the flow configuration and the DNSs in the properties of the external forcing and the run time, the results are generally consistent in terms of $\beta \leqslant 1$. However, there is significant spread between the data points for experimental and numerical results alike. Similarly, experimentally measured values for the Kolmogorov constant C_K resulted in consistent values $C_K \simeq 1.6$ for different flow configurations albeit with considerable scatter in the data (Sreenivasan 1995). Furthermore, the highest-resolution DNS of homogeneous isotropic turbulence carried out so far revealed a difference between the numerically and experimentally measured values of C_K, with $C_K = 1.8 \pm 0.1$ obtained numerically (Ishihara *et al.* 2016). In summary, for both β and C_K the difference between the measured values is not large enough to support non-universality, neither is the statistical error small enough to disprove it.

Any question of universality, however, must be taken in the appropriate context, which is here that of 'equilibrium turbulence' (Batchelor 1953; Vassilicos 2015), where the maximal inertial flux Π equals ε. There are many flow configurations where the relation $\Pi = \varepsilon$ is violated, such as in decaying turbulence and for unsteady flows (Bos *et al.* 2007; Valente & Vassilicos 2012; Valente *et al.* 2014; Vassilicos 2015; Bos & Rubinstein 2017), where the variation in the Taylor surrogate L/U^3 describes variations of Π and not of ε (McComb *et al.* 2010; Valente *et al.* 2014). In such cases, the value of β may differ from that for equilibrium turbulence for reasons connected with the unsteadiness of the flow. Therefore the present paper is only concerned with homogeneous turbulence maintained in a statistically stationary state by large-scale external forcing.

Recent numerical results suggest that β depends on the number density of stagnation points in the large-scale flow field, i.e. on topological details of the large-scale flow (Goto & Vassilicos 2009). A dependence of the inertial flux (and thus ε) on the topology of the flow field had already been inferred by Moffatt (1985, 2014) through the effect of kinetic helicity on the nonlinear structure of the Navier-Stokes equations. The kinetic helicity is the L^2-inner product $(\boldsymbol{u}, \boldsymbol{\omega})$ of the velocity field $\boldsymbol{u}$ and the vorticity field $\boldsymbol{\omega} = \nabla \times \boldsymbol{u}$. It is not only a measure of the alignment between velocity and vorticity and a conserved quantity under Euler evolution, but also a topological invariant of the Euler equations related to the linking number of infinitesimal vortex lines (Moffatt 1969, 1985). Since an alignment between $\boldsymbol{u}$ and $\boldsymbol{\omega}$ results in a depletion of nonlinearity, regions of high helicity have been conjectured to be related to low levels of dissipation (Moffatt 2014). Similar conclusions concerning a depletion of energy transfer in presence of strong helicity had already been obtained by Kraichnan (1973) based on interactions of helical Fourier modes. Although helicity is an inviscid invariant, it does not have a coercive effect on the dynamics compared to e.g. the enstrophy in two-dimensional turbulence, because it is in general not sign definite. However, once the helicity is made sign definite through a projection operation, the energy cascade direction is reversed (Biferale *et al.* 2012, 2013) and the corresponding helically projected Navier-Stokes equations admit globally regular solutions (Biferale & Titi 2013).

Owing to its aforementioned connection to nonlinear Navier-Stokes dynamics and

its relevance to atmospheric physics (Lilly 1986), the effect of helicity has been studied in a variety of turbulent flows, including homogeneous isotropic turbulence (Chen *et al.* 2003*a*,*b*; Kessar *et al.* 2015; Stepanov *et al.* 2015; Gledzer & Chkhetiani 2015; Sahoo & Biferale 2015; Alexakis 2017), rotating turbulence (Mininni & Pouquet 2010*a*,*b*) and the atmospheric boundary layer (Deusebio & Lindborg 2014). However, the dependence of β on the helicity of the external force has never been investigated analytically or numerically. The present work aims to close this gap by providing both analytical estimates and numerical measurements of β as a function of the helicity of the forcing. In view of universality, helicity is also a convenient tool to distinguish between forcing functions while keeping parameters such as characteristic length and time scales the same.

Mathematically rigorous bounds for the dissipation rate have been derived from the existence of weak solutions of the Navier-Stokes equations for a variety of wall-bounded flows (Howard 1972; Busse 1978; Doering & Constantin 1994; Nicodemus *et al.* 1998; Kerswell 1998) as well as for the case of periodic boundary conditions and sufficiently smooth forcing functions (Childress *et al.* 2001; Foias *et al.* 2001; Doering & Foias 2002). Concerning the dimensionless dissipation coefficient β, Doering & Foias (2002) derived the following bound

$$\beta \leqslant \beta_\infty + \frac{\gamma}{\mathrm{Re}_f} \,, \tag{1.1}$$

where β_∞ and γ are constants depending on the forcing function (Doering & Foias 2002), and Re_f a Reynolds number defined with respect to the characteristic length scale of the external force. The value of the upper bound has been calculated and compared to experimental and numerical data for different flow configurations (Doering *et al.* 2003; Doering & Petrov 2005; Rollin *et al.* 2011). In all cases the upper bound is approximately an order of magnitude larger than the measured value. However, for generalisations of Kolmogorov flow where the effect of different forcing scales has been studied, the predicted variation of β_∞ is in qualitative agreement with numerically obtained values for β (Rollin *et al.* 2011). In view of universality, following the arguments by Frisch (1995), a dependence of β on the forcing band can indeed be expected.

The aim of this paper is to demonstrate that the upper bound theory also captures the *quantitative* dependence of β_∞ as a function of the helicity of the force independently of its time dependence, in the sense that it is able to predict non-universal relative values of β_∞ in agreement with numerical results. For this purpose bounds for forces which differ in their level of helicity and dimensionality are calculated explicitly, and the upper bound theory is extended to include time-dependent forces. The main results of this analysis are: (i) Helical forces lead to lower bounds for β_∞ compared to non-helical forces. This supports the rationale of Moffatt (1985, 2014) that a high level of helicity should inhibit the energy cascade. (ii) Dynamic forces lead to larger bounds than static forces, where the value of the bound depends now also on the characteristic time scale of the force. A comparison to DNS data then shows that the relative dependence of β_∞ on helicity as predicted by the upper bound theory is in good qualitative and quantitative agreement with numerically measured values of β, and the results are independent of the dynamical details of the force. The relative values of β_∞ are related to the relative values of the Kolmogorov constant C_K in order to predict a qualitative and quantitative dependence of C_K on the helicity of the forcing. Finally, the effect helical forces on the Smagorinsky constant in LES is discussed.

This paper is organised as follows. The necessary mathematical concepts are introduced in sec. 2 alongside the statement of the main problem and a summary of the derivation

of the general upper bound by Doering & Foias (2002). This method is applied to time-dependent forces in section 3, while the helicity dependence of static forces is studied in section 4, including implications for the Kolmogorov constant and the Smagorinsky constant in LES in sections 4.2 and 4.3, respectively. A comparison to DNS data is carried out in section 5. The main results are summarised and discussed in section 6.

2. Background

The Navier-Stokes equations are considered on a three-dimensional domain $\Omega = [0, L]^3$ with periodic boundary conditions

$$\partial_t \boldsymbol{u} = -\frac{1}{\rho}\nabla P - (\boldsymbol{u}\cdot\nabla)\boldsymbol{u} + \nu\Delta\boldsymbol{u} + \boldsymbol{f} \ , \tag{2.1}$$

$$\nabla\cdot\boldsymbol{u} = 0 \ , \tag{2.2}$$

where $\boldsymbol{u}(\cdot, t) \in L^2(\Omega)$ is the velocity field, ν the kinematic viscosity, P the pressure, $\boldsymbol{f}(\cdot, t) \in L^2(\Omega)$ an external mechanical force and ρ the density which is set to unity for convenience. The initial conditions are assumed to be sufficiently well-behaved to allow weak solutions, i.e solutions of the corresponding integral equation where all derivatives act on test functions, which are by definition infinitely many times differentiable. In the following such weak solutions are considered and any occurrence of a derivative acting on $\boldsymbol{u}$ is understood as shorthand notation for $\boldsymbol{u}$ integrated against the derivative of a smooth test function.

Leray (1934) established the existence of weak solutions of the Navier-Stokes equation in three spatial dimensions for square-integrable sufficiently regular initial conditions and external forces (Ladyshenskaya 1969; Constantin & Foias 1988; Doering & Gibbon 1995; Foias *et al.* 2001). These weak solutions are square integrable and the existence result is valid for the three-dimensional torus as well as for the whole space $\mathbb{R}^3$ with the appropriate boundary conditions. Regarding the external force, sufficiently regular usually means that the Fourier coefficients of the force are square summable (or square integrable, in case of $\mathbb{R}^3$) at all times and

$$\sup_{t\geqslant 0} ||(-\Delta)^{-1/2}\boldsymbol{f}||_2^2 = L^3 \sup_{t\geqslant 0} \sum_{\boldsymbol{k}\neq 0} \frac{1}{|\boldsymbol{k}|^2}|\hat{\boldsymbol{f}}(\boldsymbol{k}, t)|^2 < \infty \ . \tag{2.3}$$

Furthermore, the forces must be solenoidal at all times.

For static forces Doering & Foias (2002) derived an upper bound on ε from weak solutions by decomposing the force $\boldsymbol{f}$ into an amplitude $f_0 \in \mathbb{R}$ and a shape function $\boldsymbol{\phi} \in L^2([0, 1]^3)$, such that

$$\boldsymbol{f}(\boldsymbol{x}) = f_0\boldsymbol{\phi}(\boldsymbol{x}/L_f) \ , \tag{2.4}$$

where L_f is the characteristic scale at which the force is acting. The shape function is further restricted by the requirements $||\boldsymbol{\phi}||_2 = 1$ and $||\nabla(-\Delta)^{-M}\boldsymbol{\phi}||_\infty < \infty$ for some $M \in \mathbb{N}$. Such M can always be found, with the minimum requirement for $\boldsymbol{\phi} \in L^2([0, 1]^3)$ being $M > 1$. A bound for ε was then derived from the energy inequality

$$\varepsilon(t) = \nu||\nabla\boldsymbol{u}||_2^2 \leqslant (\boldsymbol{f}, \boldsymbol{u}) \leqslant f_0||\boldsymbol{\phi}||_2 \ ||\boldsymbol{u}||_2 \ , \tag{2.5}$$

by taking the inner product of the Navier-Stokes equations with $(-\Delta)^{-M}\boldsymbol{f}$ and integrating over the volume where several integrations by parts need to be carried out such that all derivatives act on the force instead of on the velocity field and the resulting inner products are bounded from above using the Cauchy-Schwarz and Hölder inequalities.

Finally the long-time average $\langle\cdot\rangle_t$ is taken †, resulting in

$$f_0 \leqslant \frac{\|\nabla(-\Delta)^{-M}\boldsymbol{\phi}\|_\infty\langle\|\boldsymbol{u}\|_2\rangle_t^2}{L_f\|(-\Delta)^{-M/2}\boldsymbol{\phi}\|_2^2} + \frac{\nu\|(-\Delta)^{-M+1}\boldsymbol{\phi}\|_2\langle\|\boldsymbol{u}\|_2\rangle_t}{L_f^2\|(-\Delta)^{-M/2}\boldsymbol{\phi}\|_2^2} \ . \tag{2.6}$$

Substitution of the upper bound for f_0 into Eq. (2.5) and subsequent rearrangement then yields the following upper bound for β

$$\beta = \beta[\boldsymbol{\phi}](\mathrm{Re}_f) \equiv \frac{\varepsilon L_f}{U^3} \leqslant \beta_\infty + \frac{\gamma}{\mathrm{Re}_f} \ , \tag{2.7}$$

where $U = \langle||\boldsymbol{u}||_2^2\rangle_t^{1/2}$ and

$$\beta_\infty = \beta_\infty[\boldsymbol{\phi}] \equiv \frac{\|\nabla(-\Delta)^{-M}\boldsymbol{\phi}\|_\infty\|\boldsymbol{\phi}\|_2}{\|(-\Delta)^{-M/2}\boldsymbol{\phi}\|_2^2} \quad \text{and} \quad \gamma = \gamma[\boldsymbol{\phi}] \equiv \frac{\|(-\Delta)^{-M+1}\boldsymbol{\phi}\|_2\|\boldsymbol{\phi}\|_2}{\|(-\Delta)^{-M/2}\boldsymbol{\phi}\|_2^2} \ , \tag{2.8}$$

hence both β_∞ and γ are functionals of the shape function $\boldsymbol{\phi}$. Here, it is important to observe that unlike β_∞, γ depends only on space-averaged quantities and is therefore fully described by the (spatial) regularity of the shape function, while β_∞ is dominated by its local structure. The latter is brought about through β_∞ depending on the L^∞-norm of the shape function, which involves single-point values.

3. Time-dependent forces

The first task is to extend the results of Doering & Foias (2002) to time-dependent forces. If, as above, the inner product of all terms in the Navier-Stokes equation with $(-\Delta)^{-M}\boldsymbol{f}$ is taken, an extra term arises on the left-hand side which does not necessarily vanish in the long-time average

$$\begin{aligned}-\langle((-\Delta)^{-M}\partial_t f_i, u_i)\rangle_t = \langle(u_i, u_j\partial_j(-\Delta)^{-M}f_i)\rangle_t + \nu\langle((-\Delta)^{-M}f_i, \Delta u_i)\rangle_t \\ + \langle((-\Delta)^{-M}f_i, f_i)\rangle_t \ .\end{aligned} \tag{3.1}$$

The main obstacle for an estimation of β for time-dependent forces thus lies in that the new term on the left-hand side of Eq. (3.1) may not be bounded. This would occur were $\boldsymbol{f}$ rough in time. In order to proceed, $\boldsymbol{f}$ could either be assumed to be temporally sufficiently well behaved, i.e. $\boldsymbol{f}(\boldsymbol{x},\cdot) \in H^1([0,\infty))$, or convoluted with a filter kernel $G^\tau \in H^\infty([0,\infty))$ such that $(G^\tau * \boldsymbol{f})(\boldsymbol{x},\cdot) \in H^1([0,\infty))$. The latter approach introduces a time scale τ, which will turn out to be useful in the assessment of the resulting upper bound of β. Therefore, instead of using Eq. (3.1), before taking the inner products the force is smoothed by convolution with G^τ, resulting in

$$\begin{aligned}-\langle((-\Delta)^{-M}\partial_t(G^\tau * f_i), u_i)\rangle_t = \langle(u_i, u_j\partial_j(-\Delta)^{-M}G^\tau * f_i)\rangle_t + \nu\langle((-\Delta)^{-M}G^\tau * f_i, \Delta u_i)\rangle_t \\ + \langle((-\Delta)^{-M}G^\tau * f_i, f_i)\rangle_t \ .\end{aligned} \tag{3.2}$$

After some intermediate steps involving estimates of G^τ and its time derivative which can be found in Appendix A, one obtains

$$\beta_\infty = \frac{\langle||\nabla(-\Delta)^{-M}\boldsymbol{\phi}||_\infty\rangle_t\langle||\boldsymbol{\phi}||_2\rangle_t}{\langle||(-\Delta)^{-M/2}\boldsymbol{\phi}||_2^2\rangle_t} + \frac{\omega_f}{\omega}\frac{\langle||(-\Delta)^{-M}\boldsymbol{\phi}||_2\rangle_t\langle||\boldsymbol{\phi}||_2\rangle_t}{\langle||(-\Delta)^{-M/2}\boldsymbol{\phi}||_2^2\rangle_t} \ , \tag{3.3}$$

with $\omega = U/L_f = 1/T$ denoting the frequency corresponding to the forcing-scale eddy turnover time and $\omega_f \leqslant 1/\tau$ the characteristic frequency of the smoothed forcing, with τ

† The time average can be put on rigorous mathematical grounds by considering statistical solutions to the Navier-Stokes equations (Foias *et al.* 2001).

being set by the filter width. For static forcing $\omega_f = 0$, the time averages in the definitions of the coefficients β_∞ and γ can be omitted, and the forms of β_∞ and γ as in Eq. (2.8) are recovered. Dynamic forces can thus be expected to yield larger bounds due to the extra term in Eq. (2.8) which occurs only for time-dependent forces. This may imply that the bound becomes less tight for dynamic forces but it could also indicate that the value of β for dynamic forces may be larger than for static forces. This point will be further assessed in Section 5 using results from numerical simulations.

4. Dependence of β on the helicity of the force

In order to highlight the influence of the helicity of the force on the upper bound of β, the coefficients β_∞ and γ given in Eq. (2.8) are calculated explicitly for static forcing functions which differ in the helicity of their corresponding shape functions. For this purpose we consider two shape functions which are eigenfunctions of the curl operator

$$\boldsymbol{\phi}^{(1)} = \frac{1}{\sqrt{A^2+B^2+C^2}} \begin{pmatrix} A\sin 2\pi z + C\cos 2\pi y \\ B\sin 2\pi x + A\cos 2\pi z \\ C\sin 2\pi y + B\cos 2\pi x \end{pmatrix} . \tag{4.1}$$

and

$$\boldsymbol{\phi}^{(-1)} = \frac{1}{\sqrt{A^2+B^2+C^2}} \begin{pmatrix} A\cos 2\pi z + C\sin 2\pi y \\ B\cos 2\pi x + A\sin 2\pi z \\ C\cos 2\pi y + B\sin 2\pi x \end{pmatrix} . \tag{4.2}$$

where $A, B, C \in \mathbb{R}$ and $||\boldsymbol{\phi}^{(\pm 1)}||_2 = 1$, see Appendix B for further details. These shape functions are by construction fully helical, as their relative helicity is given by

$$\rho_{\boldsymbol{\phi}^{(\pm 1)}} = \frac{(\boldsymbol{\phi}^{(\pm 1)}, \nabla \times \boldsymbol{\phi}^{(\pm 1)})}{\|\nabla \times \boldsymbol{\phi}^{(\pm 1)}\| \|\boldsymbol{\phi}^{(\pm 1)}\|} = \pm \frac{\|\boldsymbol{\phi}^{(\pm 1)}\|_2^2}{\|\boldsymbol{\phi}^{(\pm 1)}\|_2^2} = \pm 1 , \tag{4.3}$$

as $\boldsymbol{\phi}^{(\pm 1)}$ are eigenfunctions of the curl operator with eigenvalues one and minus one, respectively. The latter also implies that $\boldsymbol{\phi}^{(1)}$ and $\boldsymbol{\phi}^{(-1)}$ are orthogonal with respect to the L^2 inner product. A shape function $\boldsymbol{\phi}^{(\rho_\phi)}$ of arbitrary relative helicity ρ_ϕ is then constructed by suitable linear combination of $\boldsymbol{\phi}^{(1)}$ and $\boldsymbol{\phi}^{(-1)}$

$$\phi^{(\rho_\phi)} = \sqrt{\frac{1+\rho_\phi}{2}}\phi^{(1)} + \sqrt{\frac{1-\rho_\phi}{2}}\phi^{(-1)} . \tag{4.4}$$

Force functions $\boldsymbol{f}^{(\rho_f)}$ of a given relative helicity $\rho_f \equiv \rho_\phi$ are then constructed according to equation (2.4). A further assessment of the effect of dimensionality can be carried out by setting one or two of the coefficients A, B or C to zero.

Before calculating the values of $\beta_\infty^{(\rho_f)}$ corresponding to $\boldsymbol{f}^{(\rho_f)}$, certain topological and geometrical properties of the two functions corresponding to the cases $\rho_f = 1$ and $\rho_f = 0$ are discussed. The Navier-Stokes equations subject to a fully helical force $\boldsymbol{f}^{(1)}$ with $f_0^{(1)} = \nu k_f^2$ have an exact 'laminar' solution. (Here, laminar refers to vanishing nonlinearity, and does not necessarily imply a layered structure.) This solution is $\boldsymbol{f}^{(1)}$ itself, it is known as Arnol'd-Beltrami-Childress (ABC) flow (Childress 1970; Dombre *et al.* 1986) and has been studied extensively in connection with dynamo action in magnetohydrodynamics (MHD). Depending on the values of A, B and C, $\boldsymbol{f}^{(1)}$ has up to eight stagnation points (Dombre *et al.* 1986). In contrast, a 'laminar' flow given by $\boldsymbol{f}^{(0)}$ has only the trivial stagnation points $x = y = z = 0$ and $x = y = z = \pi$ independently of the values of A, B and C, see Appendix D. The two functions also differ in terms of their symmetry groups,

while the symmetry group of $\boldsymbol{f}^{(1)}$ is isomorphic to $\mathbb{Z}_2 \times \mathbb{Z}_2 \times \mathbb{Z}_2$ (Dombre *et al.* 1986), that of $\boldsymbol{f}^{(0)}$ is isomorphic to $\mathbb{Z}_2 \times \mathbb{Z}_2$, see Appendix D.

A dependence of the coefficients $\beta_\infty^{(\rho_f)}$ and $\gamma^{(\rho_f)}$ on ρ_f is now obtained by straightforward analytical evaluation of the norms on the right-hand side of (2.8). Since $\boldsymbol{\phi}^{(\rho_f)}$ consist of trigonometric functions they satisfy $(-\Delta)^{-M}\boldsymbol{\phi}^{(\rho_f)} = \boldsymbol{\phi}^{(\rho_f)}/(2\pi)^{2M}$, and the L^2-norm of their gradients is calculated directly

$$\begin{aligned}\|(-\Delta)^{-M/2}\boldsymbol{\phi}^{(\rho_f)}\|_2^2 &= ((-\Delta)^{-M/2}\boldsymbol{\phi}^{(\rho_f)}, (-\Delta)^{-M/2}\boldsymbol{\phi}^{(\rho_f)}) \\ &= (\boldsymbol{\phi}^{(\rho_f)}, (-\Delta)^{-M}\boldsymbol{\phi}^{(\rho_f)}) = \frac{(\boldsymbol{\phi}^{(\rho_f)}, \boldsymbol{\phi}^{(\rho_f)})}{(2\pi)^{2M}} = \frac{1}{(2\pi)^{2M}} \ . \end{aligned} \tag{4.5}$$

The evaluation of $\|\nabla(-\Delta)^{-M}\boldsymbol{\phi}^{(\rho_f)}\|_\infty = \|\nabla\boldsymbol{\phi}^{(\rho_f)}\|_\infty/(2\pi)^{2M}$ proceeds explicitly by using the definition of the L^∞ norm

$$\|\nabla\boldsymbol{\phi}^{(\rho_f)}\|_\infty = \sup_{\boldsymbol{x}\in[0,1]^3} |\nabla\boldsymbol{\phi}^{(\rho_f)}| = \sup_{\boldsymbol{x}\in[0,1]^3} (\partial_i\phi_j^{(\rho_f)}\partial_i\phi_j^{(\rho_f)})^{\frac{1}{2}}, \tag{4.6}$$

where a sum over repeated indices is implied. Evaluating the last term in Eq. (4.6) for $\boldsymbol{\phi}^{(\rho_f)}$ results in

$$\|\nabla\boldsymbol{\phi}^{(\rho_f)}\|_\infty = 2\pi\left(\sqrt{\frac{1+\rho_f}{2}} + \sqrt{\frac{1-\rho_f}{2}}\right) \ , \tag{4.7}$$

see Appendix B for further details. The values for the norms are now combined according to Eq. (2.8), leading to

$$\beta_\infty^{(\rho_f)} = \sqrt{2}\pi\left(\sqrt{1-\rho_f} + \sqrt{1+\rho_f}\right) \ , \tag{4.8}$$

$$\gamma^{(\rho_f)} = (2\pi)^2 \ . \tag{4.9}$$

From Eq. (4.8) one obtains the following expression for the helicity dependence of the asymptote normalised by the zero-helicity value $\beta_\infty^{(0)}$

$$\frac{\beta_\infty^{(\rho_f)}}{\beta_\infty^{(0)}} = \frac{\sqrt{1+\rho_f} + \sqrt{1-\rho_f}}{2} \leqslant 1 \ , \tag{4.10}$$

which implies $\beta_\infty^{(\rho_f)}/\beta_\infty^{(0)} \in [1/\sqrt{2}, 1]$. That is, a helical large-scale force results in a lower estimate for the non-dimensional total asymptotic energy dissipation rate compared to a non-helical force, provided the forces are acting on the same single length scale. In contrast, the approach to the asymptote is independent of ρ_f following Eq. (4.9). Equation (4.10) is the first main result of this paper.

Since β_∞ is also a measure of the inertial flux of the turbulent cascade for statistically steady turbulence in the infinite-Reynolds-number limit, it implies that a high level of helicity has a detrimental effect on the energy cascade. Thus the results obtained by the upper bound theory are qualitatively in accord with the predictions by Moffatt concerning the effect of helicity on turbulence dynamics. The latter prediction, however, was concerned with the helicity of the flow and not the forcing, which is assessed here. It is known that large-scale helicity injection does not lead to highly helical flows, as mirror symmetry is quickly recovered at successively smaller scales (Chen *et al.* 2003*a*; Deusebio & Lindborg 2014; Kessar *et al.* 2015). Hence Eq. (4.10) could perhaps best be viewed in terms of a large-scale control problem: through an adjustment in the helicity of the forcing it may be possible to regulate the value of the inertial flux across scales without having to invoke a depletion of nonlinearity in regions of high helicity at intermediate or small scales.

4.1. *Variational approach for bidirectional static forces*

The values for the bounds given in Eqs. (4.8) and (4.9) do not depend on the dimensionality of the force because setting either one or two of the coefficients A, B or C in Eqs. (4.1) and (4.2) to zero does not alter the results. However, for forces depending on only one spatial coordinate the upper bounds can be improved through a generalisation of the variational method developed by (Doering *et al.* 2003) for shear flows with unidirectional force, where the streamwise component of the Navier-Stokes equations is projected on a suitable multiplier function. The resulting upper bound on β is then evaluated by minimisation over the set of multiplier functions (Doering *et al.* 2003; Rollin *et al.* 2011).

This method is not applicable for three-dimensional (3-D) forces, as an average over the direction of the force is taken. In order to apply it to the present case, set $A = B = 0$ such that $\boldsymbol{\phi} = (\phi_x(y), 0, \phi_z(y))$ for $y \in [0,1]$, where ϕ_x and ϕ_y are periodic functions on $[0,1]$. Let $\boldsymbol{\psi} = (\psi_x(y), 0, \psi_z(y))$ be a function whose second derivative $\boldsymbol{\Psi} = (\partial_y\psi_x, 0, \partial_y\psi_z)$ is square integrable (i.e. $\boldsymbol{\psi} \in H^2([0,1])$) and which satisfies $(\boldsymbol{\psi}, \boldsymbol{\phi}) \neq 0$. Similar to Doering *et al.* (2003), consider $\boldsymbol{\Phi} \equiv (-\partial_y^{-1}\phi_x, 0, -\partial_y^{-1}\phi_z)$, such that $(\boldsymbol{\Psi}, \boldsymbol{\Phi}) = (\partial_y\boldsymbol{\psi}, -\partial_y\boldsymbol{\phi}) = (\boldsymbol{\psi}, \boldsymbol{\phi})$. Following the procedure outlined in Sec. 2, *i.e.* taking the inner product of the Navier-Stokes equation with $\boldsymbol{\psi}$ and integrating by parts, one obtains

$$\beta \leqslant \min_{\psi} \max_{\tilde{\boldsymbol{u}}} \left(\frac{(\tilde{\boldsymbol{u}}, (\tilde{\boldsymbol{u}}\cdot\nabla)\boldsymbol{\psi})(\tilde{\boldsymbol{u}}, \boldsymbol{\phi})}{(\boldsymbol{\Psi}, \boldsymbol{\Phi})} + \frac{(\tilde{\boldsymbol{u}}, \partial_y\boldsymbol{\Psi})(\tilde{\boldsymbol{u}}, \boldsymbol{\phi})}{\mathrm{Re}_f(\boldsymbol{\Psi}, \boldsymbol{\Phi})} \right) , \tag{4.11}$$

where $\tilde{\boldsymbol{u}} = (u_x, u_y, u_z) = \boldsymbol{u}/U$. The next step consists of a maximisation over all divergence-free normalised vector fields $\tilde{\boldsymbol{u}}$. The inner products in the numerators on the right-hand side of Eq. (4.11) are considered separately, beginning with the inertial term

$$\begin{aligned}
(\tilde{\boldsymbol{u}}, (\tilde{\boldsymbol{u}}\cdot\nabla)\boldsymbol{\psi}) &= \int_\Omega d\boldsymbol{x}\ u_x u_y \partial_y\psi_x(y) + u_z u_y \partial_y\psi_z(y) = \int_\Omega d\boldsymbol{x}\ u_x u_y \Psi_x(y) + u_z u_y \Psi_z(y) \\
&= \int_\Omega d\boldsymbol{x}\ \tilde{\boldsymbol{u}}\cdot u_y\boldsymbol{\Psi}(y) \leqslant \|\boldsymbol{\Psi}\|_\infty \|u_y\tilde{\boldsymbol{u}}'\|_1 = \|\boldsymbol{\Psi}\|_\infty \int_\Omega d\boldsymbol{x}\ |u_y| |\sqrt{u_x^2 + u_z^2}| \\
&\leqslant \|\boldsymbol{\Psi}\|_\infty \int_\Omega d\boldsymbol{x}\ |u_y|(|u_x| + |u_z|) \leqslant \frac{\|\boldsymbol{\Psi}\|_\infty}{2} \int_\Omega d\boldsymbol{x}\ u_x^2 + u_z^2 + 2u_y^2 \\
&= \frac{\|\boldsymbol{\Psi}\|_\infty}{2} \left(1 + \int_\Omega d\boldsymbol{x}\ u_y^2 \right) ,
\end{aligned} \tag{4.12}$$

where $\tilde{\boldsymbol{u}}' = (u_x, 0, u_z)$, while the monotonicity of the square-root was used in $\sqrt{u_x^2 + u_z^2} \leqslant \sqrt{(|u_x| + |u_z|)^2}$ and the triangle inequality in $|u_x u_y| \leqslant (u_x^2 + u_y^2)/2$. For the viscous term, one obtains

$$|(\tilde{\boldsymbol{u}}, \Delta^{1/2}\boldsymbol{\Psi})| = |(\tilde{\boldsymbol{u}}', \Delta^{1/2}\boldsymbol{\Psi})| \leqslant \|\Delta^{1/2}\boldsymbol{\Psi}\|_2 \|\tilde{\boldsymbol{u}}'\|_2 = \|\Delta^{1/2}\boldsymbol{\Psi}\|_2 \left(\|u_x\|_2^2 + \|u_z\|_2^2 \right)^{1/2} , \tag{4.13}$$

since $\Psi_y = 0$. The last term to evaluate is

$$\begin{aligned}
|(\tilde{\boldsymbol{u}}, \Delta^{1/2}\boldsymbol{\Phi})| = |(\tilde{\boldsymbol{u}}, \boldsymbol{\phi})| &= \left| \int_\Omega d\boldsymbol{x}\ \phi_x u_x + \phi_z u_z \right| \leqslant \left| \int_\Omega d\boldsymbol{x}\ \phi_x u_x \right| + \left| \int_\Omega d\boldsymbol{x}\ \phi_z u_z \right| \\
&\leqslant \|\phi_x\|_2 \|u_x\|_2 + \|\phi_z\|_2 \|u_z\|_2 \leqslant \|u_x\|_2 + \|u_z\|_2 ,
\end{aligned} \tag{4.14}$$

since the normalisation $\|\boldsymbol{\phi}\|_2 = 1$ implies $\|\phi_x\|_2 \leqslant 1$ and $\|\phi_z\|_2 \leqslant 1$. Following the procedure of Doering *et al.* (2003), set

$$\xi^2 = \|u_x\|_2^2 + \|u_z\|_2^2 , \tag{4.15}$$

such that

$$\|u_y\|_2^2 = 1 - \|u_x\|_2^2 + \|u_z\|_2^2 = 1 - \xi^2 \ , \tag{4.16}$$

$$(\|u_x\|_2 + \|u_z\|_2)^2 = \xi^2 + 2\|u_x\|_2\|u_z\|_2 \leqslant 2\xi^2 \ , \tag{4.17}$$

where the inequality $2|xy| \leqslant x^2 + y^2$ was used again. Now Eq. (4.11) can be written as

$$\beta \leqslant \min_{\boldsymbol{\psi}} \frac{1}{(\boldsymbol{\Psi},\boldsymbol{\Phi})} \max_{\xi\in[0,1]} \left(\frac{\xi(2-\xi^2)}{\sqrt{2}} \|\boldsymbol{\Psi}\|_\infty + \frac{\|\Delta^{1/2}\boldsymbol{\Psi}\|_2}{\mathrm{Re}_f} \sqrt{2}\xi^2 \right) . \tag{4.18}$$

For $\mathrm{Re}_f \to \infty$ the maximisation over ξ results in $\xi = \sqrt{2/3}$ and $\max_{\xi\in[0,1]} \xi(2-\xi^2)/\sqrt{2} = 4/\sqrt{27}$, such that

$$\beta_\infty \leqslant \min_{\boldsymbol{\psi}} \max_{\tilde{\boldsymbol{u}}} \frac{(\tilde{\boldsymbol{u}}, (\tilde{\boldsymbol{u}}\cdot\nabla)\boldsymbol{\psi})(\tilde{\boldsymbol{u}}, \Delta^{1/2}\boldsymbol{\Phi})}{(\boldsymbol{\Psi},\boldsymbol{\Phi})} \leqslant \min_{\boldsymbol{\psi}} \frac{1}{(\boldsymbol{\Psi},\boldsymbol{\Phi})} \frac{4\|\boldsymbol{\Psi}\|_\infty}{\sqrt{27}} \ . \tag{4.19}$$

The remaining minimisation over the multiplier $\boldsymbol{\Psi}$ proceeds by minor modifications of the method devised by Doering *et al.* (2003); Rollin *et al.* (2011). For this purpose, consider

$$(\boldsymbol{\Psi},\boldsymbol{\Phi}) = (\boldsymbol{\Psi}, (\boldsymbol{\Phi} - \boldsymbol{C})) \leqslant \|\boldsymbol{\Psi}\|_\infty \|(\boldsymbol{\Phi} - \boldsymbol{C})\|_1 \ , \tag{4.20}$$

for any constant vector $\boldsymbol{C} = (C_x, C_y, C_z)$, as ψ_x and ψ_z are periodic functions with zero mean. The inequality is saturated if $\boldsymbol{\Phi} - \boldsymbol{C}$ and $\boldsymbol{\Psi}$ are fully aligned, that is if $\boldsymbol{\Psi}$ is a unit vector pointing in the direction of $\boldsymbol{\Phi} - \boldsymbol{C}$. The minimum over $\boldsymbol{\Psi}$ in Eq. (4.19) is therefore realised for

$$\min_{C_x,C_z} \int_0^1 dy |\boldsymbol{\Phi} - \boldsymbol{C}| \ , \tag{4.21}$$

from which the following conditions for $\boldsymbol{C}$ realising the minimum become

$$\begin{aligned} 0 &= \frac{\partial}{\partial C_x} \int_0^1 dy \ \sqrt{(\Phi_x - C_x)^2 + \Phi_z - C_z)^2} \Big|_{C_{x,z}=C_{x,z}^{\min}} \\ &= \int_0^1 \frac{\Phi_x - C_x^{\min}}{\sqrt{(\Phi_x - C_x^{\min})^2 + (\Phi_z - C_z^{\min})^2}} \ , \end{aligned} \tag{4.22}$$

$$\begin{aligned} 0 &= \frac{\partial}{\partial C_z} \int_0^1 dy \ \sqrt{(\Phi_x - C_x)^2 + \Phi_z - C_z)^2} \Big|_{C_{x,z}=C_{x,z}^{\min}} \\ &= \int_0^1 \frac{\Phi_z - C_z^{\min}}{\sqrt{(\Phi_x - C_x^{\min})^2 + (\Phi_z - C_z^{\min})^2}} \ . \end{aligned} \tag{4.23}$$

For the periodic functions $\boldsymbol{\phi}^X$ considered here $C_x^{\min} = C_z^{\min} = 0$ satisfies these conditions. Hence the final result for the minimax problem in the limit $\mathrm{Re}_f \to \infty$ is

$$\beta_\infty \leqslant \min_{\boldsymbol{\psi}} \max_{\tilde{\boldsymbol{u}}} \frac{(\tilde{\boldsymbol{u}}, (\tilde{\boldsymbol{u}}\cdot\nabla)\boldsymbol{\psi})(\tilde{\boldsymbol{u}}, \Delta^{1/2}\boldsymbol{\Phi})}{(\boldsymbol{\Psi},\boldsymbol{\Phi})} \leqslant \frac{4}{\sqrt{27}} \frac{1}{\int_0^1 dy |\partial_y^{-1}\boldsymbol{\phi}|} \ . \tag{4.24}$$

The final step consists of an evaluation of the integral on the right-hand side of Eq. (4.24) for the static shape functions $\boldsymbol{\phi}^{(\rho_f)}$ considered here for $A = B = 0$, resulting in

$$\frac{\beta_\infty^{(\rho_f)}}{\beta_\infty^{(0)}} = \left(\frac{\pi}{2} \int_0^1 dy \ \sqrt{1 - \sqrt{1-\rho_f^2}\sin(4\pi y)} \right)^{-1} \geqslant \frac{2\sqrt{2}}{\pi} \simeq 0.9003 \ , \tag{4.25}$$

see Appendix C for the calculation. The ratio between the dissipation factors is now larger compared to the previous estimate in Eq. (4.10) because the minimisation procedure replaces the L^∞-norm of $\nabla^{-1}\boldsymbol{\phi}$ with essentially the L^1-norm. For the helical shape

functions $\boldsymbol{\phi}^{(\pm 1)}$ one thus expects no effect from the minimisation owing to the fact that unlike for $\nabla\boldsymbol{\phi}^{(\rho_f)}$ with $|\rho_f| < 1$, the L^∞-norm of $\nabla\boldsymbol{\phi}^{(\pm 1)}$ equals the L^1-norm.

4.2. *Implications for the value of the Kolmogorov constant*

The dimensionless dissipation coefficient has a direct relation to the Kolmogorov constant C_K, since the relation $\varepsilon = \beta U^3/L_f$ can be viewed as a special case of Kolmogorov scaling formally extended to the turbulence production range (Lumley 1992). More precisely, if u_ℓ is the magnitude of the velocity-field fluctuations at scale ℓ in the inertial range, then Kolmogorov-scaling of the energy spectrum implies $\varepsilon\ell/u_\ell^3 \sim C_K^{-2/3} = const.$ Formally extending this scaling to the production range, where $\ell = L_f$ and $u_\ell \simeq U$ would yield the desired result, which by consequence implies $C_K \sim \beta^{-2/3}$. However, this is only justified if L_f lies in the inertial range, which is not the case at finite Reynolds number. That is, the argument can only be applied in the formal limit of infinite Reynolds number, where the inertial range extends through all $k \neq 0$. This limit corresponds to replacing β with β_∞, which yields

$$C_K \sim \beta_\infty^{-2/3} \ . \tag{4.26}$$

It is important to point out that this argument does not take into account that ε can vary locally, a point already made by Lumley (1992). Therefore, the scaling given in Eq. (4.26) can only be viewed as an approximation. Equation (4.26) can now be used to obtain the ratio of Kolmogorov constants for helical and non-helical forces from the ratio $\beta_\infty^{(\rho_f)}/\beta_\infty^{(0)}$

$$\frac{C_K^{(\rho_f)}}{C_K^{(0)}} = \left(\frac{\beta_\infty^{(\rho_f)}}{\beta_\infty^{(0)}}\right)^{-\frac{2}{3}} \ . \tag{4.27}$$

For 3-D static forces, where the minimisation procedure cannot be applied, one obtains the following explicit dependence of the relative value of the Kolmogorov constant on the helicity of the external forcing from Eq. (4.10) and Eq. (4.27)

$$\frac{C_K^{(\rho_f)}}{C_K^{(0)}} = \left(\sqrt{\frac{1+\rho_f}{8}} + \sqrt{\frac{1-\rho_f}{8}}\right)^{-2/3} \leqslant 2^{1/3} \ . \tag{4.28}$$

For shear flows where the minimisation procedure does apply, one obtains

$$\frac{C_K^{(\rho_f)}}{C_K^{(0)}} = \left(\frac{\pi}{2}\int_0^1 dy\ \sqrt{1-\sqrt{1-\rho_f^2}\sin\left(4\pi y\right)}\right)^{2/3} \leqslant \frac{\pi^{2/3}}{2} \ . \tag{4.29}$$

The estimates hence result in the following range of values for the two extreme cases

$$1.07 \simeq \frac{\pi^{2/3}}{2} \leqslant \frac{C_K^{(1)}}{C_K^{(0)}} \leqslant 2^{1/3} \simeq 1.26 \ . \tag{4.30}$$

4.3. *Implications for the Smagorinsky constant in LES*

As mentioned in the Introduction, the value of β is not only of theoretical interest because of its relation to the parametrisation of the subgrid scales in LES, such as for the Smagorinsky model (Smagorinsky 1963). The aim of LES is to simulate only the motion at large and intermediate scales, while the effect of the small scales is modelled. More precisely, let $\overline{\boldsymbol{u}}$ be the velocity field $\boldsymbol{u}$ convoluted with a filter kernel G^Δ, where Δ is the characteristic filter width: $\overline{\boldsymbol{u}} = G^\Delta * \boldsymbol{u}$. The evolution of the filtered field is then

governed by the following equations

$$\partial_t \overline{\boldsymbol{u}} = -\frac{1}{\rho}\nabla \overline{P} - (\overline{\boldsymbol{u}}\cdot\nabla)\overline{\boldsymbol{u}} + \nu\Delta\overline{\boldsymbol{u}} + \boldsymbol{f} - \nabla\cdot\boldsymbol{\tau}^{\Delta} \ , \tag{4.31}$$

$$\nabla\cdot\overline{\boldsymbol{u}} = 0 \ , \tag{4.32}$$

where $\tau_{ij}^{\Delta} = \overline{u_i u_j} - \overline{u}_i\overline{u}_j$ is the subgrid-scale stress tensor and we assume $\Delta < L_f$ such that $\overline{\boldsymbol{f}} = \boldsymbol{f}$. Since τ_{ij}^{Δ} is not closed in term of $\overline{\boldsymbol{u}}$, it must be modelled. The Smagorinsky model for τ_{ij}^{Δ} is based on the observation that the mean energy flux in 3-D turbulence proceeds from the large scales to the small scales, it models the deviatoric part of τ_{ij}^{Δ} as

$$\tau_{ij}^{\Delta} = 2(c_S\Delta)^2\sqrt{\overline{s}_{ij}\overline{s}_{ij}}\overline{s}_{ij} \ , \tag{4.33}$$

where $\overline{s}_{ij} = (\partial_i\overline{u}_j + \partial_j\overline{u}_i)$ is the resolved-scale strain tensor and c_S the Smagorinsky constant, which is an adjustable parameter. Since the subgrid-scale energy transfer at scale Δ is given by

$$\Pi^{\Delta} = \overline{s}_{ij}\tau_{ij}^{\Delta} \ , \tag{4.34}$$

the Smagorinsky model leads to a *pointwise* non-negative subgrid-scale energy flux

$$\Pi^{\Delta} = \overline{s}_{ij}2(c_S\Delta)^2\sqrt{\overline{s}_{ij}\overline{s}_{ij}}\overline{s}_{ij} = 2(c_S\Delta)^2\sqrt{\overline{s}_{ij}\overline{s}_{ij}}\overline{s}_{ij}\overline{s}_{ij} \geqslant 0 \ . \tag{4.35}$$

The Smagorinsky constant can be related to β_∞ using the estimate by Lilly (1967) for the value of the Smagorinsky constant for statistically steady homogeneous isotropic turbulence, $c_S = (3C_K/2)^{-4/3}/\pi$, in combination with Eq. (4.26)

$$c_S = \frac{\left(\frac{2}{3C_K}\right)^{4/3}}{\pi} \sim \beta_\infty^{1/2} \ . \tag{4.36}$$

In terms of the dependence of c_S on ρ_f, the above scaling results in a relative relation between c_S and β_∞

$$\frac{c_S(\rho_f)}{c_S(0)} = \left(\frac{\beta_\infty(\rho_f)}{\beta_\infty(0)}\right)^{1/2} \ , \tag{4.37}$$

which implies the following dependence of c_S on the relative helicity of the forcing

$$\frac{c_S(\rho_f)}{c_S(0)} = \left(\frac{\sqrt{1+\rho_f}+\sqrt{1-\rho_f}}{2}\right)^{1/2} \ , \tag{4.38}$$

for isotropic forcing and

$$\frac{c_S(\rho_f)}{c_S(0)} = \left(\frac{\pi}{2}\int_0^1 dy\ \sqrt{1-\sqrt{1-\rho_f^2}\sin(4\pi y)}\right)^{-1/2} \ , \tag{4.39}$$

for shear flows. In summary, the values of c_S decrease for increasing ρ_f, and in case of a strongly helical force the usual value of $c_S \simeq 0.17$ (Lilly 1967) of the Smagorinsky constant should be decreased according to the corresponding values of β_∞. Since the eddy viscosity $\nu_E = 2(c_S\Delta)^2\sqrt{\overline{s}_{ij}\overline{s}_{ij}}$ depends quadratically on c_S, it depends linearly on β_∞, which results in a decrease of at least 10% in case of strongly helical forcing.

In the context of subgrid-scale modelling, the effect of helicity is usually included through an extra model term (Yokoi & Yoshizawa 1993; Li *et al.* 2006; Baerenzung *et al.* 2008; Inagaki *et al.* 2017), leading to an additional diffusion mechanism in the model. Here, the modelling of the unresolved inertial dynamics as a dissipative loss is the same and only the amount of dissipation is changed depending on the helicity of the

external force. Li *et al.* (2006) investigated different subgrid-scale models in *a-priori* and *a-posteriori* analyses of isotropic helical turbulence. The effect of the newly introduced terms in helical subgrid-scale models was found to be quite small. Interestingly, the dynamic Smagorinsky model, where the model coefficient is adjusted in response to the flow, performed best in comparison with DNS data. An *a-posteriori* analysis of the static Smagorinsky model with c_S adjusted as discussed here could be of interest in this context.

5. Numerical simulations

Equations (2.1)-(2.2) are solved numerically in a three-dimensional periodic domain of length $L_{box} = 2\pi$ using a fully de-aliased pseudospectral code. In order to assess the influence of helicity, dimensionality and time dependence of the forcing on the value of the dimensionless dissipation coefficient, DNSs were carried out using different forcing functions, including the static forces constructed using the shape functions given in Eqs. (4.2) and (4.1) according to Eq. (4.4). Simulation series carried out using these static shape functions are identified by the label S, followed by the dimensionality of the force and the relative helicity level. Here, the label 1D2C refers to one-dimensional two-component shape functions where e.g. $A = B = 0$ while 3D refers to three-dimensional forces with $A = B = C$. Since the different implementations of time-dependent forcing have little effect on the measured value for β (Bos *et al.* 2007), it is sufficient to consider only one type of time-dependent forcing for comparison to the static forces. The time-dependent forcing was given by a Gaussian distributed $\delta(t)$-correlated stochastic process, which is particularly suited to the present investigation because it gives optimal control over both kinetic energy and helicity injection rates. The helicity of the random force is set by expanding the Fourier modes $\hat{\boldsymbol{f}}$ of the force field in a basis consisting of eigenfunctions of the curl operator (Constantin & Majda 1988; Waleffe 1992), i.e. into positively and negatively helical modes, such that the helicity of the force can be adjusted exactly at each wavevector (Brandenburg 2001). Simulation series carried out using dynamic forcing are identified by the labels D1 and D2, followed by the helicity level of the force. All simulations of series S and D2 are carried out using 256^3 collocation points, while simulations of series D1 were carried out using 512^3 collocation points. The force always acts the large scales $L_f = \pi/k_f$, i.e. at wavenumbers $k_f \leqslant 2.5$ for runs of series D1 and at $k_f = 1$ for all other simulations. For case D2, the random force is equivalent to a phase-shifted ABC-flow with randomly chosen phases and values of A, B and C.

All runs are carried out with a fixed time step dt chosen by the Courant-Friedrichs-Lewy criterion, where in case of white-in-time forcing dt determines the characteristic frequency of the force by $\omega_f = 2\pi/dt$. According to Eq. (3.3), white-in-time forcing should therefore lead to a maximal weighting of the extra contribution to β_∞ originating from the time dependence of the forcing compared to forces with larger correlation times. Measurements are taken after the simulations have reached a statistically stationary state, all simulations are evolved for more than 25 large-eddy turnover times in stationary state. It has been pointed out by Bos *et al.* (2007) that averaging intervals of more than 10 large-eddy turnover times are necessary in order to obtain accurate values of β. The long runtime of the simulations is particularly important for the present study in order to distinguish the helicity dependence of the measured values of β from the statistical error, resulting in a need to compromise between achievable runtime and resolution. A summary of the numerical details including information on the small-scale resolution and measured values

Run id	N	Re	Re_λ	ε	U	L	β	δ_β	β_L	δ_{β_L}	ρ	ρ_f	$k_{max}\eta$	$\frac{\nu}{10^3}$	t/T
D1-0	512	842	162	0.11	0.61	0.97	1.56	0.03	0.48	0.01	0.004	0.0	1.27	0.705	29
D1-1	512	846	168	0.08	0.57	1.05	1.35	0.05	0.45	0.02	0.15	1.0	1.39	0.705	27
D2-0	256	584	151	0.09	0.68	1.55	0.88	0.06	0.433	0.03	0.001	0.0	1.37	1.8	111
D2-025	256	532	142	0.06	0.61	1.56	0.86	0.04	0.427	0.02	0.04	0.25	1.48	1.8	100
D2-05	256	538	146	0.06	0.61	1.59	0.84	0.05	0.42	0.03	0.08	0.5	1.50	1.8	102
D2-075	256	535	146	0.05	0.59	1.64	0.77	0.04	0.40	0.02	0.14	0.75	1.57	1.8	98
D2-1	256	616	167	0.06	0.65	1.71	0.68	0.05	0.37	0.03	0.17	1.0	1.50	1.8	106
S3D-0	256	611	143	0.02	0.41	1.50	0.95	0.02	0.45	0.01	-0.0008	0.0	1.26	1.0	54
S3D-025	256	600	142	0.018	0.40	1.52	0.92	0.02	0.447	0.01	0.07	0.25	1.30	1.0	60
S3D-05	256	619	148	0.016	0.39	1.58	0.85	0.02	0.426	0.01	0.11	0.5	1.34	1.0	58
S3D-075	256	629	154	0.014	0.386	1.63	0.78	0.03	0.40	0.01	0.14	0.75	1.39	1.0	54
S3D-1	256	614	156	0.01	0.37	1.67	0.72	0.02	0.38	0.01	0.16	1.0	1.46	1.0	65
S1D2C-0	256	645	151	0.56	1.26	1.54	0.89	0.03	0.43	0.01	0.01	0.0	1.24	3.0	115
S1D2C-025	256	584	143	0.41	1.14	1.54	0.88	0.02	0.43	0.01	0.07	0.25	1.36	3.0	168
S1D2C-05	256	608	150	0.37	1.13	1.62	0.80	0.02	0.41	0.01	0.11	0.5	1.40	3.0	167
S1D2C-075	256	615	155	0.31	1.10	1.68	0.73	0.02	0.39	0.01	0.15	0.75	1.49	3.0	157
S1D2C-1	256	630	162	0.26	1.08	1.76	0.65	0.02	0.36	0.01	0.18	1.0	1.53	3.0	162

TABLE 1. Specifications of the numerical simulations. N denotes the number of grid points in each Cartesian coordinate, Re the Reynolds number with respect to the rms velocity U, the integral scale L and the kinematic viscosity ν, Re_λ the Taylor-scale Reynolds number, ε the dissipation rate, $\beta = \varepsilon L_f/U^3$ the dimensionless dissipation rate, $\beta_L = \varepsilon L/U^3$ the dimensionless dissipation rate with respect to L, δ_β and δ_{β_L} the respective standard errors, ρ the relative kinetic helicity, ρ_f the relative helicity of the forcing, η the Kolmogorov microscale, k_{max} the highest resolved wavenumber, $T = L/U$ the large-eddy turnover time, and t/T the steady-state run time in units of T. The values given for ε, U, L and ρ are ensemble averages, with the ensemble consisting of snapshots taken at intervals of T in order to obtain statistically independent samples. The identifiers D and S refer to dynamic and static forces, respectively. The two sets of simulations using static forces differ in the dimensionality of the force as indicated by the labels 3D and 1D2C.

of ε, U, L and β is given in Tbl. 1. For comparison purposes with results given in the literature for isotropic turbulence, where $\beta_L = \varepsilon L/U^3$, with L being the integral scale, is measured instead of $\beta = \varepsilon L_f/U^3$, values of β_L are also provided in the table. For the same reason, U is calculated as $U = \sqrt{2E/3}$, where E is the time-averaged kinetic energy per unit volume.

5.1. *Comparison between numerical and analytical results*

A comparison between the values of the rigorous bounds given in Eqs. (4.8) and (4.25) and the measured values given in table 1 shows that the measured values are considerably smaller than the corresponding estimates. The range of values for the non-helical 3-D forces $0.43 \leqslant {\beta_L}^{(0)} \leqslant 0.49$ obtained from the present DNSs are consistent with existing data from the literature for 3-D isotropic turbulence (Wang *et al.* 1996; Kaneda *et al.* 2003; Gotoh *et al.* 2002; Donzis *et al.* 2005; Yeung *et al.* 2012; McComb *et al.* 2015; Yeung *et al.* 2015; Ishihara *et al.* 2016), and the analytically obtained estimates differ by an order of magnitude from the measured values. Such a discrepancy between the measured value and the rigorous estimate has also been obtained for a particular type of

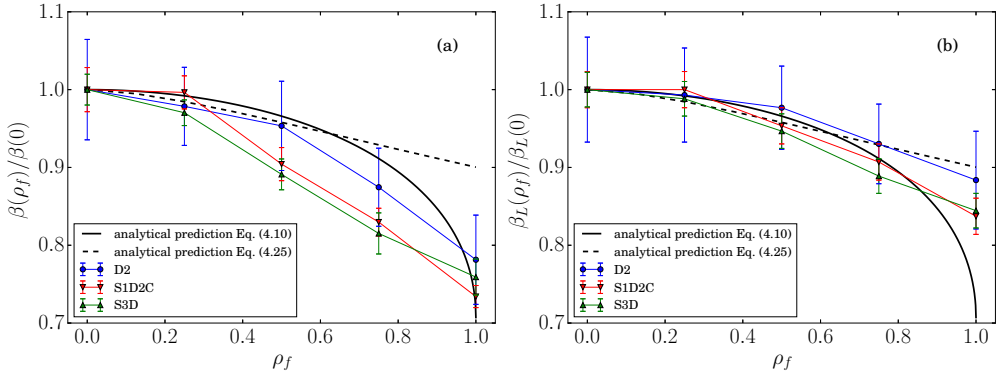

FIGURE 1. (Colour) Value of β as a function of ρ_f normalised by its value at $\rho_f = 0$ from datasets D2, S3D and S1D2C compared to the analytical predictions in Eqs. (4.10) and (4.25). (a): $\beta = \varepsilon L_f/U^3$, (b): $\beta_L = \varepsilon L/U^3$, where L is the integral scale.

dynamic forcing (Doering & Petrov 2005), given by

$$\hat{\boldsymbol{f}}(\boldsymbol{k},t) = \begin{cases} (\varepsilon/2E_f)\hat{\boldsymbol{u}}(\boldsymbol{k},t) & \text{for} \quad 0 < |\boldsymbol{k}| \leqslant k_f; \\ 0 & \text{otherwise} , \end{cases} \tag{5.1}$$

where $\hat{\boldsymbol{f}}(\boldsymbol{k},t)$ is the Fourier transform of the force and E_f the total energy contained in the forcing band. The rigorous bound derived by Doering & Petrov (2005) resulted in $\beta_\infty = 4\pi\sqrt{\frac{3}{5}} \simeq 9.73$, which could be tightened to $\beta_\infty = 2\sqrt{2}\pi$ assuming Kolmogorov scaling for the energy spectrum, *i.e.* interestingly to the same value as $\beta_\infty^{(0)}$ obtained here for the static 3-D force.

Figure 1 presents a comparison of values for $\beta^{(\rho_f)}/\beta^{(0)}$ (Fig. 1(a)) and $\beta_L^{(\rho_f)}/\beta_L^{(0)}$ (Fig. 1(b)) obtained from datasets D2, S3D and S1D2C and the analytical predictions of Eq. (4.10) and Eq. (4.25). As can be seen from the figure, the measured values are in broad agreement between the different datasets despite the lack of isotropy in case 1D2C and the dynamical nature of the forcing in case D2. Symmetries specific to the choice $A = B = C$ in case S3D have therefore little or no influence on the value of β. Furthermore, the functional dependence of the ratios $\beta^{(\rho_f)}/\beta^{(0)}$ and $\beta_L^{(\rho_f)}/\beta_L^{(0)}$ on ρ_f is consistent with the analytical predictions. This implies that although the upper bounds are by an order of magnitude higher than the measured values, there is a good agreement between the analytical and the numerical results concerning the ratio $\beta^{(\rho_f)}/\beta^{(0)}$, which in the limit $\mathrm{Re} \to \infty$ is predicted to follow Eq. (4.10) for 3-D forces and Eq. (4.25) for shear flows. Differences between the ρ_f-dependence of β and β_L originate from a ρ_f-dependence of the integral scale, which is discussed briefly in Sec. 5.3.

The effect of finite Reynolds number on the measurements can be quantified through the conventionally band-forced runs D1-0 and D1-1. For this purpose, it is useful to consider the empirical formula obtained by a least-squares fit to a dataset of β_L resulting from DNSs of stationary homogeneous isotropic turbulence maintained with the dynamic forcing specified in Eq. (5.1) for $k_f \leqslant 2.5$ (McComb *et al.* 2015)

$$\beta_L^{(0)} = 0.47 + \frac{18.9}{\mathrm{Re}} , \tag{5.2}$$

which yields $\beta_L(\mathrm{Re} = 834) = 0.49$ in good agreement with the measured value for run

D1-0 shown in table 1. For run D1-1 the same equation is considered after adjusting the value of the asymptote according to the aforementioned estimates

$$\beta_L^{(1)} = 0.42 + \frac{18.9}{\mathrm{Re}}\ , \tag{5.3}$$

which results in $\beta_L(\mathrm{Re} = 846) = 0.45$, again in good agreement with the measured value for run D1-1 shown in table 1. Hence the ratio 0.9 of the asymptotes and a helicity-independent approach to the asymptotes is consistent with the data.

Concerning a possible influence of the time dependence of the forcing on the value of β_∞, the comparison of values for β obtained from runs D2 and S3D shown in table 1 demonstrates that the value of β is comparable between the dynamically and the statically forced simulations, provided the forces act at the same length scales. Furthermore, the ratio $\beta^{(\rho_f)}/\beta^{(0)}$ appears to be largely unaffected by the time dependence of the forcing as can be seen in Fig. 1. That is, the dynamical details of the forcing have little influence on the value of β and possibly also on that of the asymptote β_∞. Note that the measured values of β for the dynamically forced simulations D1-0 and D1-1 are higher than those obtained from D2-0 and D2-1, despite the larger Reynolds number which most probably results from differences in the range of wavenumbers the force is applied in. The dependence of β on the width of the forcing band was studied analytically and numerically for Kolmogorov flow by Rollin *et al.* (2011). The analytical estimates suggested an increase of β_∞ with the width of the forcing band, which was confirmed by DNS results. The behaviour observed here is consistent with these results, as runs of series D2 were forced at $k_f = 1$ in order to enable a like-for-like comparison to the statically forced series S3D runs, while runs of series D1 were forced more conventionally in the wavenumber band $1 \leqslant k_f \leqslant 2.5$ in order to compare with results in the literature.

In summary, not only the qualitative but more importantly the relative quantitative helicity dependence of the measured values of β is in good agreement with the helicity dependence of the upper bounds. Moreover, this dependence of β on the helicity of the forcing appears to be independent of its dynamical features.

5.2. *Kolmogorov constant*

Concerning the Kolmogorov constant C_K, recent numerical measurements (Ishihara *et al.* 2016) showed that accurate numerical measurements of C_K require Taylor-scale Reynolds numbers $\mathrm{Re}_\lambda \geqslant 700$ and hence very high resolution DNSs. Furthermore, numerical results at $\mathrm{Re}_\lambda = 2297$ requiring 12288^3 collocation points revealed a difference between the numerically and experimentally measured values of C_K, with $C_K = 1.8 \pm 0.1$ obtained numerically (Ishihara *et al.* 2016) and $C_K \simeq 1.6$ obtained from experimental data for several flow configurations (Sreenivasan 1995). The value of the Kolmogorov constant thus appears still to be an open question, and DNSs at much higher Reynolds numbers than those carried out in the present paper are necessary to test any predicted variations for the Kolmogorov constant such as those presented here.

5.3. *Further observations*

As can be seen from table 1, the integral scale is slightly larger for helical forces with $L^{(0)}/L^{(1)} \simeq 0.9$ consistently in all test cases. Although a proper interpretation of integral scale is perhaps ambiguous as the largest scales are dominated by the forcing in the present simulations, the measurements suggest that helically forced flows consist

of larger eddies. This is expected by the depletion of nonlinearity in regions of high helicity (Moffatt 1985, 2014). Although mirror symmetry is generally quickly recovered at the small scales, (Kraichnan 1973; Chen *et al.* 2003*a*; Deusebio & Lindborg 2014; Kessar *et al.* 2015), the high level of helicity at the large scales diminishes the forward flux of kinetic energy and hence the efficiency of the kinetic energy cascade leading to less generation of small-scale turbulent fluctuations (Moffatt 2014). In the decaying case, the same effect results in a delay in the onset of the decay for non-zero helicity (Polifke & Shtilman 1989). A similar conclusion can be achieved by noting that despite comparable large-scale and Taylor-scale Reynolds numbers, the helically forced turbulent flows are all better resolved, implying that the Kolmogorov microscale is larger for the helically forced simulations compared to the non-helically forced runs.

A reduction in the formation of small-scale structures with increasing ρ_f is reminiscent of drag-reducing processes in wall-bounded flows. More precisely, at a given value of U a decrease in ε in homogeneous turbulence corresponds to a decrease in the wall shear stress in wall-bounded flows. Such an effect is indeed obtained with increasing ρ_f as shown in Fig. 2, where ε is presented as a function of U. It can be quantified through the measure

$$R(\rho_f) = \frac{\beta^{(0)} - \beta^{(\rho_f)}}{\beta^{(0)}} \,, \tag{5.4}$$

which is equals the ratio of the corresponding dissipation rates at fixed U. From the analytical and numerical results, one obtains $R(\rho_f = 1) \simeq 30\%$.

6. Conclusions

Upper bounds for the dimensionless dissipation coefficient β have been evaluated analytically depending on the relative helicity ρ_f of the external forcing. The main results were: (i) helical forces lead to a lower estimate of the flux compared to a non-helical force, (ii) a time-dependent force result in a larger estimate of the flux compared to a static force owing to an extra term appearing in the upper bound. The calculated values of $\beta^{(\rho_f)}$ were subsequently compared with values obtained from DNSs which differed in the helicity level, the time dependence and the dimensionality of the forcing. The agreement between the theoretically and numerically obtained values is good *concerning the ratio* $\beta^{(\rho_f)}/\beta^{(0)}$ despite a difference of an order of magnitude between theory and simulation results concerning the single quantities $\beta^{(\rho_f)}$. Time-dependent forces do not lead to larger values of $\beta^{(\rho_f)}$ compared to static forces, and the value of the ratio $\beta^{(\rho_f)}/\beta^{(0)}$ is comparable between static and dynamic forces. This indicates that the extra term that appears in the upper bounds for dynamic forces arises from an analytical difficulty in deriving tight estimates for dynamic forces and does not carry any relevant information concerning the value of the energy flux.

In summary, even though the actual estimates are not very tight, the upper bound theory captures well the dependence of helicity, i.e. of a topological property, of the force on the forward flux of kinetic energy not only qualitatively but also quantitatively. This result is robust under differences in the dynamical properties of the forcing. The forward flux of energy across the scales can thus be described by the spatial regularity and the helicity of the force, which in principle can be adjusted by the experimenter. Hence it may be possible to devise a particular type of force which controls this forward flux of energy, thus leading to a suppression or enhancement of turbulence and thus of e.g. nonlinear mixing or drag. The present results also suggest that detailed knowledge of the topological

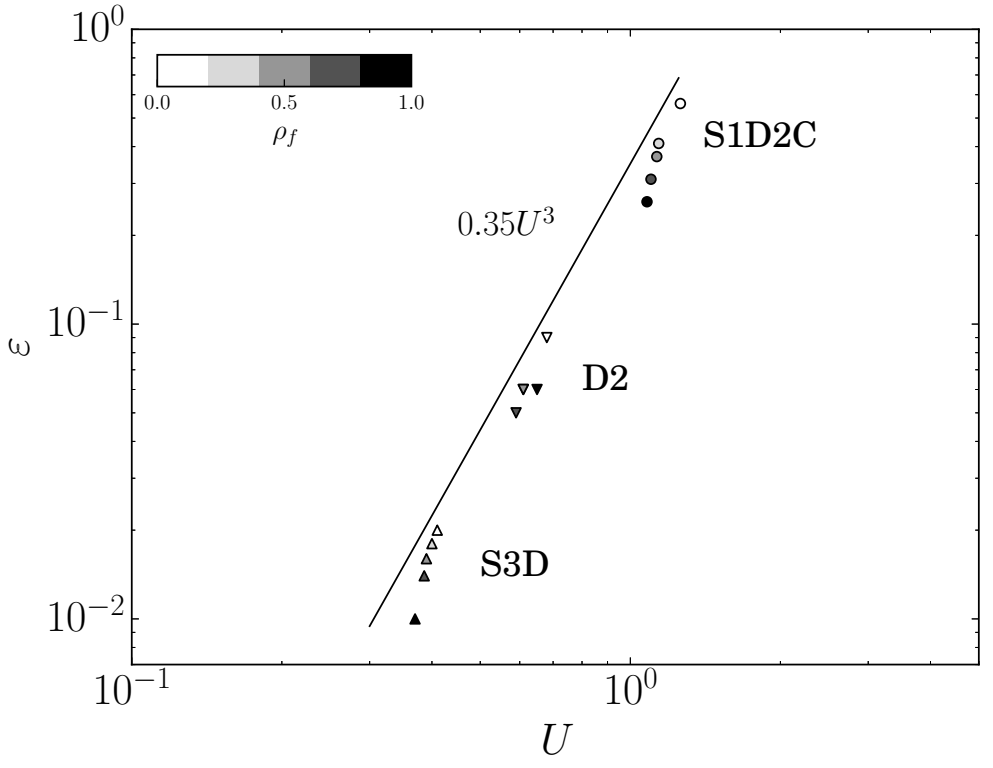

FIGURE 2. Value of ε as a function of U on a logarithmic scale for datasets S1D2C, D2 and S3D. The solid line shows the scaling $\varepsilon \sim U^3$, which corresponds to a fixed value of β and L_f. The grey-shading indicates different values of ρ_f. A trend can be observed: For a fixed value of U, the dissipation rate decreases with increasing forcing helicity.

properties of a naturally occurring external force field may enable some predictions about the level of turbulence in a flow. Since β is related to the model coefficient relating the turbulent kinetic energy to its dissipation rate in the k-ε model and to the eddy viscosity in LES, the present results may also be useful in practical applications concerned with flows subject to helical forces such as in atmospheric physics.

Acknowledgements

Helpful discussions and suggestions by B. Eckhardt, C. Doering, L. Biferale and M. Buzzicotti are gratefully acknowledged. Part of the numerical work was carried out during a postdoctoral position at the University of Rome 'Tor Vergata' funded through the European Union's Seventh Framework Programme (FP7/2007-2013) under grant agreement no. 339032.

Appendix A. Time-dependent forcing

Let $\boldsymbol{f} = f_0 g(t) \boldsymbol{\phi}(\boldsymbol{x}/L_f)$ and consider a Gaussian filter function G^τ, with characteristic time scale τ. From the energy inequality one obtains an upper bound for ε by the same boundedness argument as in the case of static forcing

$$\varepsilon \leqslant f_0 \langle g \rangle_t \|\boldsymbol{\phi}\|_2 \langle \|\boldsymbol{u}\|_2 \rangle_t \ . \tag{A 1}$$

The next step proceeds similar to the static case by taking the inner product of all terms in the Navier-Stokes equations with $G^\tau * (-\Delta)^{-M}\boldsymbol{f}$, and the arguments concerning the spatial dependence of the force are exactly the same. Each term in equation (3.2) is now considered separately, beginning with the new term on the left-hand side

$$-\langle((-\Delta)^{-M}\partial_t(G^\tau * f_i), u_i)\rangle_t = -\langle((-\Delta)^{-M}\partial_t G^\tau * f_i, u_i)\rangle_t = \left\langle \frac{\tau^2}{t^3}((-\Delta)^{-M} G^\tau * f_i, u_i)\right\rangle_t , \tag{A 2}$$

which results in

$$\langle((-\Delta)^{-M}\partial_t(G^\tau * f_i), u_i)\rangle_t \leqslant f_0 \left| \left\langle \frac{\tau^2}{t^3} G^\tau * g \right\rangle_t \right| \|(-\Delta)^{-M}\boldsymbol{\phi}\|_2 \langle \|\boldsymbol{u}\|_2\rangle_t L_f^{2M} . \tag{A 3}$$

For the terms on the right-hand side one obtains

$$\langle(u_i, u_j\partial_j(-\Delta)^{-M} G^\tau * f_i)\rangle_t \leqslant f_0 |\langle G^\tau * g\rangle_t| \|\nabla(-\Delta)^{-M}\boldsymbol{\phi}\|_\infty (\langle\|\boldsymbol{u}\|_2\rangle_t)^2 L_f^{2M-1} \tag{A 4}$$

$$\nu\langle((-\Delta)^{-M} G^\tau * f_i, \Delta u_i)\rangle_t \leqslant f_0 |\langle G^\tau * g\rangle_t| \|(-\Delta)^{-M+1}\boldsymbol{\phi}\|_2 (\langle\|\boldsymbol{u}\|_2\rangle_t)^2 L_f^{2M-2} \tag{A 5}$$

$$\langle((-\Delta)^{-M} G^\tau * f_i, f_i)\rangle_t = f_0^2 \langle(G^\tau * g)g\rangle_t \|(-\Delta)^{-M/2}\boldsymbol{\phi}\|_2^2 L_f^{2M} , \tag{A 6}$$

where in the last line $\langle(G^\tau * g)g\rangle_t > 0$. Hence one obtains the following upper bound

$$f_0 \leqslant U \frac{|\langle G^\tau * g\rangle_t|}{\langle(G^\tau * g)g\rangle_t} \left(\frac{\|(-\Delta)^{-M}\boldsymbol{\phi}\|_2}{\|(-\Delta)^{-M/2}\boldsymbol{\phi}\|_2^2} + \frac{U}{L_f} \frac{\|\nabla(-\Delta)^{-M}\boldsymbol{\phi}\|_\infty}{\|(-\Delta)^{-M/2}\boldsymbol{\phi}\|_2^2} + \frac{\nu}{L_f^2} \frac{\|(-\Delta)^{-M+1}\boldsymbol{\phi}\|_2}{\|(-\Delta)^{-M/2}\boldsymbol{\phi}\|_2^2} \right) , \tag{A 7}$$

which substituted into Eq. (A 1) yields after some rearrangement a bound on β

$$\beta \leqslant \frac{|\langle G^\tau * g\rangle_t| \langle g\rangle_t}{\langle(G^\tau * g)g\rangle_t} \left(\frac{|\langle(\tau^2/t^3)G^\tau * g\rangle_t|}{|\langle G^\tau * g\rangle_t|} \frac{L_f}{U} \frac{\|(-\Delta)^{-M}\boldsymbol{\phi}\|_2 \|\boldsymbol{\phi}\|_2}{\|(-\Delta)^{-M/2}\boldsymbol{\phi}\|_2^2} + \frac{\|\nabla(-\Delta)^{-M}\boldsymbol{\phi}\|_\infty \|\boldsymbol{\phi}\|_2}{\|(-\Delta)^{-M/2}\boldsymbol{\phi}\|_2^2} + \frac{1}{\mathrm{Re}} \frac{\|(-\Delta)^{-M+1}\boldsymbol{\phi}\|_2 \|\boldsymbol{\phi}\|_2}{\|(-\Delta)^{-M/2}\boldsymbol{\phi}\|_2^2} \right) . \tag{A 8}$$

The summand on the right-hand side of the above inequality can be further approximated by considering

$$\lim_{t\to\infty} (\tau^2/t^3) G^\tau * g = 0 , \tag{A 9}$$

since both G^τ and g are bounded, and

$$\lim_{t\to 0} (\tau^2/t^3) G^\tau * g = 0 , \tag{A 10}$$

since $G^\tau = \exp(-\tau^2/t^2)$ goes to zero faster than any power for $t \to 0$. The average value is thus dominated by the integrand at $t = \tau$ and can be approximated as

$$|\langle(\tau^2/t^3)G^\tau * g\rangle_t| \simeq |\langle G^\tau * g\rangle_t|/\tau , \tag{A 11}$$

such that with the definitions $\omega_f = 1/\tau$ and $\omega = U/L_f$ one obtains Eq. (3.3).

Appendix B. Evaluation of norms for shape functions $\boldsymbol{\phi}^{\rho_f}$.

The terms to evaluate explicitly are $\|\nabla(-\Delta)^{-M}\boldsymbol{\phi}^{\rho_f}\|_\infty$ and $\|\boldsymbol{\phi}^{(\rho_f)}\|^2$. We first establish that the fully helical shape functions are normalised to unity

$$\|\boldsymbol{\phi}^{(\pm1)}\|_2^2 = \frac{1}{|[0,1]^3|}\frac{1}{A^2+B^2+C^2}\int_{[0,1]^3} dx\ dy\ dz\ \Big(B^2(\sin(2\pi x)^2+\cos(2\pi x)^2) + C^2(\sin(2\pi y)^2+\cos(2\pi y)^2)+A^2(\sin(2\pi z)^2+\cos(2\pi z)^2)\Big) = 1\ . \quad \text{(B 1)}$$

Since $\boldsymbol{\phi}^{(\pm1)}$ are eigenfunctions of the curl operator, they are also orthogonal with respect to the L^2-inner product, i.e. $(\boldsymbol{\phi}^{(1)},\boldsymbol{\phi}^{(-1)})=0$. For a shape function with fractional relative helicity we therefore obtain

$$\begin{aligned}\|\phi^{(\rho_f)}\|_2^2 &= \left(\sqrt{\frac{1+\rho_f}{2}}\boldsymbol{\phi}^{(1)}+\sqrt{\frac{1-\rho_f}{2}}\boldsymbol{\phi}^{(-1)},\sqrt{\frac{1+\rho_f}{2}}\boldsymbol{\phi}^{(1)}+\sqrt{\frac{1-\rho_f}{2}}\boldsymbol{\phi}^{(-1)}\right)\\ &= \frac{1+\rho_f}{2}\|\boldsymbol{\phi}^{(1)}\|_2^2+\frac{1-\rho_f}{2}\|\boldsymbol{\phi}^{(-1)}\|_2^2 = 1\ . \end{aligned} \quad \text{(B 2)}$$

The term $\|\nabla(-\Delta)^{-M}\boldsymbol{\phi}^{(\rho_f)}\|_\infty = \|\nabla\boldsymbol{\phi}^{(\rho_f)}\|_\infty/(2\pi)^{2M}$ is calculated by first considering the gradients of the shape functions

$$\nabla\boldsymbol{\phi}^{(1)} = \frac{2\pi}{\sqrt{A^2+B^2+C^2}}\begin{pmatrix}0 & B\cos2\pi x & -B\sin2\pi x\\ -C\sin2\pi y & 0 & C\cos2\pi y\\ A\cos2\pi z & -A\sin2\pi z & 0\end{pmatrix}\ , \quad \text{(B 3)}$$

$$\nabla\boldsymbol{\phi}^{(-1)} = \frac{2\pi}{\sqrt{A^2+B^2+C^2}}\begin{pmatrix}0 & -B\sin2\pi x & B\cos2\pi x\\ C\cos2\pi y & 0 & -C\sin2\pi y\\ -A\sin2\pi z & A\cos2\pi z & 0\end{pmatrix}\ . \quad \text{(B 4)}$$

Now the L^∞-norm of $\nabla\boldsymbol{\phi}^{(\rho_f)}$ can be calculated. For this purpose, set $\alpha\equiv\sqrt{(1+\rho_f)/2}$ and $\gamma\equiv\sqrt{(1-\rho_f)/2}$, such that

$$\begin{aligned}\|\nabla\boldsymbol{\phi}^{(\rho_f)}\|_\infty &= \sup_{\boldsymbol{x}\in[0,1]^3}\left(\sum_{i,j=1}^3\partial_i\phi_j^{(\rho_f)}\partial_i\phi_j^{(\rho_f)}\right)^{\frac12} = \sup_{\boldsymbol{x}\in[0,1]^3}\left(\sum_{i,j=1}^3\left[\partial_i\left(\alpha\phi_j^{(1)}+\gamma\phi_j^{(-1)}\right)\right]^2\right)^{\frac12}\\ &= \frac{2\pi}{\sqrt{A^2+B^2+C^2}}\sup_{\boldsymbol{x}\in[0,1]^3}\Big(B^2\left[(\alpha\cos2\pi x-\gamma\sin2\pi x)^2+(\gamma\cos2\pi x-\alpha\sin2\pi x)^2\right]\\ &\quad +C^2\left[(\alpha\cos2\pi y-\gamma\sin2\pi y)^2+(\gamma\cos2\pi y-\alpha\sin2\pi y)^2\right]\\ &\quad +A^2\left[(\alpha\cos2\pi z-\gamma\sin2\pi z)^2+(\gamma\cos2\pi z-\alpha\sin2\pi z)^2\right]\Big)^{1/2}\\ &= \frac{2\pi}{\sqrt{A^2+B^2+C^2}}\sup_{\boldsymbol{x}\in[0,1]^3}\Big(B^2\left[\alpha^2+\gamma^2-4\alpha\gamma\cos2\pi x\sin2\pi x\right]\\ &\quad +C^2\left[\alpha^2+\gamma^2-4\alpha\gamma\cos2\pi y\sin2\pi y\right]+A^2\left[\alpha^2+\gamma^2-4\alpha\gamma\cos2\pi z\sin2\pi z\right]\Big)^{1/2}\ . \end{aligned} \quad \text{(B 5)}$$

Since $\sqrt{a}$ is a monotonic function for $a\in\mathbb{R}$, the supremum is realised at a point $\boldsymbol{x}=(x,y,z)\in[0,1]^3$ where each summand is maximal. This is the case for $x=y=z=1/8$ since $\cos\pi/4=1/\sqrt{2}$ and $\sin\pi/4=-1/\sqrt{2}$, such that

$$\begin{aligned}\|\nabla\boldsymbol{\phi}^{(\rho_f)}\|_\infty &= \frac{2\pi}{\sqrt{A^2+B^2+C^2}}\left((A^2+B^2+C^2)\left[\alpha^2+\gamma^2+2\alpha\gamma\right]\right)^{1/2} = 2\pi|\alpha+\gamma|\\ &= \sqrt{2}\pi\left(\sqrt{1-\rho_f}+\sqrt{1+\rho_f}\right)\ . \end{aligned} \quad \text{(B 6)}$$

Finally, one obtains

$$\|\nabla(-\Delta)^{-M}\boldsymbol{\phi}^{(\rho_f)}\|_\infty = \|\nabla\boldsymbol{\phi}^{(\rho_f)}\|_\infty/(2\pi)^{2M} = \frac{\sqrt{2}\pi\left(\sqrt{1-\rho_f}+\sqrt{1+\rho_f}\right)}{(2\pi)^{2M}} \ . \tag{B 7}$$

Appendix C. Evaluation of the integrals in Eq. (4.24) for bidirectional static forces

Consider the two static forces $\boldsymbol{\phi}^{(\pm1)}$ for $A = B = 0$. For simplicity we set $C = 1$, such that

$$-\partial_y^{-1}\boldsymbol{\phi}^{(1)} = \frac{1}{2\pi}\begin{pmatrix}-\sin 2\pi y\\ 0\\ \cos 2\pi y\end{pmatrix} \qquad \text{and} \qquad -\partial_y^{-1}\boldsymbol{\phi}^{(-1)} = \frac{1}{2\pi}\begin{pmatrix}\cos 2\pi y\\ 0\\ -\sin 2\pi y\end{pmatrix} \ , \tag{C 1}$$

such that

$$-\partial_y^{-1}\boldsymbol{\phi}^{(\rho_f)} = \sqrt{\frac{1+\rho_f}{2}}\begin{pmatrix}-\sin 2\pi y\\ 0\\ \cos 2\pi y\end{pmatrix} + \sqrt{\frac{1-\rho_f}{2}}\begin{pmatrix}\cos 2\pi y\\ 0\\ -\sin 2\pi y\end{pmatrix} \ . \tag{C 2}$$

The evaluation of the integral on the right-hand side of Eq. (4.24) proceeds by explicit calculation. For convenience, set $\alpha \equiv \sqrt{(1+\rho_f)/2}$ and $\gamma \equiv \sqrt{(1-\rho_f)/2}$, such that

$$\begin{aligned}\int_0^1 dy\ |\partial_y^{-1}\boldsymbol{\phi}^{(\rho_f)}| &= \frac{1}{2\pi}\int_0^1 dy\ \sqrt{(\alpha\cos 2\pi y - \gamma\sin 2\pi y)^2 + (\gamma\cos 2\pi y - \alpha\sin 2\pi y)^2}\\ &= \frac{1}{2\pi}\int_0^1 dy\ \sqrt{\alpha^2+\gamma^2-2\alpha\gamma\sin 4\pi y}\\ &= \frac{1}{2\pi}\int_0^1 dy\ \sqrt{1-\sqrt{1-\rho_f^2}\sin 4\pi y}\ ,\end{aligned} \tag{C 3}$$

where the integrand has no closed-form antiderivative. For the extreme cases $\rho_f = \pm1$ and $\rho_f = 0$, one obtains

$$\int_0^1 dy\ |\partial_y^{-1}\boldsymbol{\phi}^{(\pm1)}| = \frac{1}{2\pi}\int_0^1 dy\ \sqrt{(\sin 2\pi y)^2 + (\cos 2\pi y)^2} = \frac{1}{2\pi}\ , \tag{C 4}$$

$$\begin{aligned}\int_0^1 dy\ |\partial_y^{-1}\boldsymbol{\phi}^{(0)}| &= \frac{1}{2\pi}\int_0^1 dy\ \sqrt{1-\sin 4\pi y} = \frac{1}{2\pi}\int_0^1 dy\ \sqrt{(\cos 2\pi y - \sin 2\pi y)^2}\\ &= \frac{1}{2\pi}\int_0^1 dy\ \sqrt{2}|\sin(2\pi y + \pi/4)| = \frac{1}{2\pi}\int_0^1 dy\ \sqrt{2}|\sin 2\pi y| = \frac{\sqrt{2}}{\pi^2}.\end{aligned} \tag{C 5}$$

Appendix D. Stagnation points and symmetries

In this appendix we consider the stagnation points and symmetries of a flow corresponding to $\boldsymbol{\phi}^{(0)}$, i.e. given by

$$\boldsymbol{v}^{(0)} \equiv \begin{pmatrix}\dot{x}(t)\\ \dot{y}(t)\\ \dot{z}(t)\end{pmatrix} = \begin{pmatrix}A\sin 2\pi z(t) + C\sin 2\pi y(t)\\ B\sin 2\pi x(t) + A\sin 2\pi z(t)\\ C\sin 2\pi y(t) + B\sin 2\pi x(t)\end{pmatrix} \ , \tag{D 1}$$

on the periodic domain $[0,1)^3$. The stagnation points of $\boldsymbol{v}^{(0)}$ require $\boldsymbol{v}^{(0)} = 0$, however

$$\dot{x}(t) = 0 \implies A\sin 2\pi z(t) = -C\sin 2\pi y(t)\ , \tag{D 2}$$

$$\dot{z}(t) = 0 \implies B\sin 2\pi x(t) = -C\sin 2\pi y(t)\ , \tag{D 3}$$

result in $\dot{y}(t) = -2C \sin 2\pi y(t)$. Hence $\boldsymbol{v}^{(0)} = 0$ if and only if $x = y = z = 0$ or $x = y = z = \pi$. The symmetry group of $\boldsymbol{v}^{(0)}$ consists of the following four elements $\{\mathrm{id}, \sigma_1, \sigma_2, \sigma_3\}$ where id denotes the identity transformation and

$$\sigma_1(x) = -x,\ \sigma_1(y) = -y,\ \sigma_1(z) = -z,\ \sigma_1(t) = t; \tag{D 4}$$

$$\sigma_2(x) = x + \pi,\ \sigma_2(y) = y + \pi,\ \sigma_2(z) = z + \pi,\ \sigma_2(t) = t; \tag{D 5}$$

$$\sigma_3(x) = -x - \pi,\ \sigma_3(y) = -y - \pi,\ \sigma_3(z) = -z - \pi,\ \sigma_3(t) = -t. \tag{D 6}$$

Since $\sigma_3 = \sigma_1 \circ \sigma_2$, the set $\{\mathrm{id}, \sigma_1, \sigma_2, \sigma_3\}$ indeed forms a group. It is isomorphic to the direct product of the cyclic group of two elements $\mathbb{Z}_2$ with itself because $\sigma_i^2 = \mathrm{id}$ for $i \in \{1, 2, 3\}$.

REFERENCES

Alexakis, A. 2017 Helically decomposed turbulence. *J. Fluid Mech.* **812**, 752–770.

Baerenzung, J., Politano, H., Ponty, Y. & Pouquet, A. 2008 Spectral modeling of turbulent flows and the role of helicity. *Phys. Rev. E.* **77**, 046303.

Batchelor, G. K. 1953 *The theory of homogeneous turbulence*, 1st edn. Cambridge University Press, Cambridge.

Biferale, L., Musacchio, S. & Toschi, F. 2012 Inverse energy cascade in three-dimensional isotropic turbulence. *Phys. Rev. Lett.* **108**, 164501.

Biferale, L., Musacchio, S. & Toschi, F. 2013 Split Energy-Helicity cascades in three dimensional Homogeneous and Isotropic Turbulence. *J. Fluid Mech.* **730**, 309–327.

Biferale, L. & Titi, E. S. 2013 On the global regularity of a helical-decimated version of the 3D Navier-Stokes equation. *Journ. Stat. Phys* **151**, 1089–1098.

Bos, W. J. T. & Rubinstein, R. 2017 Dissipation in unsteady turbulence. *Phys. Rev. Fluids.* **2**, 022601(R).

Bos, W. J. T., Shao, L. & Bertoglio, J.-P. 2007 Spectral imbalance and the normalized dissipation rate of turbulence. *Phys. Fluids* **19**, 45101.

Brandenburg, A. 2001 The inverse cascade and nonlinear alpha-effect in simulations of isotropic helical magnetohydrodynamic turbulence. *Astrophys. J.* **550**, 824–840.

Burattini, P., Lavoie, P. & Antonia, R. 2005 On the normalised turbulence energy dissipation rate. *Phys. Fluids* **17**, 98103.

Busse, F. 1978 The optimum theory of turbulence. *Adv. Appl. Mech.* **18**, 77–121.

Chen, Q., Chen, S. & Eyink, G. L. 2003*a* The joint cascade of energy and helicity in three-dimensional turbulence. *Phys. Fluids* **15**, 361–374.

Chen, Q., Chen, S., Eyink, G. L. & Holm, D. D. 2003*b* Intermittency in the joint cascade of energy and helicity. *Phys. Rev. Lett.* **90**, 214503.

Childress, S. 1970 New solutions of the kinematic dynamo problem. *J. Math. Phys.* **11**, 3063–3076.

Childress, S., Kerswell, R.R. & Gilbert, A.D. 2001 Bounds on dissipation for NavierStokes flow with Kolmogorov forcing. *Physica D* **158** (1), 105 – 128.

Constantin, P. & Foias, C. 1988 *Navier-Stokes Equations*. University of Chicago Press.

Constantin, P. & Majda, A. 1988 The Beltrami spectrum for incompressible flows. *Commun. Math. Phys.* **115**, 435–456.

Deusebio, E. & Lindborg, E. 2014 Helicity in the Ekman boundary layer. *J. Fluid Mech.* **755**, 654–671.

Doering, C. R. & Constantin, P. 1994 Variational bounds on energy dissipation in incompressible flows: Shear flow. *Phys. Rev. E* **49**, 4087–4099.

Doering, C. R., Eckhardt, B. & Schumacher, J. 2003 Energy dissipation in body-forced plane shear flow. *J. Fluid Mech.* **494**, 275–284.

Doering, C. R. & Foias, C. 2002 Energy dissipation in body-forced turbulence. *J. Fluid Mech.* **467**, 289–306.

Doering, C. R. & Gibbon, J. D. 1995 *Applied Analysis of the Navier-Stokes Equations*. Cambridge University Press.

Doering, C. R. & Petrov, N. P. 2005 Low-wavenumber forcing and turbulent energy dissipation. In *Progress in Turbulence* (ed. M. Oberlack, J. Peinke, A. Kittel & S. Barth), *Springer Proc. Physics*, vol. 101, pp. 11–18. Springer, New York.

Dombre, T., Frisch, U., Greene, J. M., Hénon, M., Mehr, A. & Soward, A. M. 1986 Chaotic streamlines in the ABC flows. *J. Fluid Mech.* **167**, 353–391.

Donzis, D. A., Sreenivasan, K. R. & Yeung, P. K. 2005 Scalar dissipation rate and dissipative anomaly in isotropic turbulence. *J. Fluid Mech.* **532**, 199–216.

Eyink, G. L. 2003 Local 4/5-law and energy dissipation anomaly in turbulence. *Nonlinearity* **16**, 137–145.

Foias, C., Manley, O., Rosa, R. & Temam, R. 2001 *Navier-Stokes Equations and Turbulence*, *Encyclopedia of Mathematics and its Applications*, vol. 83. Cambridge University Press.

Frisch, U. 1995 *Turbulence: The Legacy of Kolmogorov*. Cambridge University Press.

Gledzer, E. B. & Chkhetiani, O. G. 2015 Inverse energy cascade in developed turbulence at the breaking of the symmetry of helical modes. *JETP Letters* **102**, 465–472.

Goto, Susumo & Vassilicos, J. C. 2009 The dissipation rate coefficient of turbulence is not universal and depends on the internal stagnation point structure. *Phys. Fluids* **21**, 035104.

Gotoh, T., Fukayama, D. & Nakano, T. 2002 Velocity field statistics in homogeneous steady turbulence obtained using a high-resolution direct numerical simulation. *Phys. Fluids* **14**, 1065.

Howard, L. N. 1972 Bounds on flow quantities. *Annu. Rev. Fluid Mech.* **4**, 473–494.

Inagaki, K., Yokoi, N. & Hamba, F. 2017 Mechanism of mean flow generation in rotating turbulence through inhomogeneous helicity. *Phys. Rev. Fluids* **2**, 114605.

Ishihara, T., Morishita, K., Yokokawa, M., Uno, A. & Kaneda, Y. 2016 Energy spectrum in high-resolution direct numerical simulations of turbulence. *Phys. Rev. Fluids* **1**, 082403(R).

Kaneda, Y., Ishihara, T., Yokokawa, M., Itakura, K. & Uno, A. 2003 Energy dissipation and energy spectrum in high resolution direct numerical simulations of turbulence in a periodic box. *Phys. Fluids* **15**, L21.

Kerswell, R.R. 1998 Unification of variational principles for turbulent shear flows: the background method of Doering-Constantin and the mean-fluctuation formulation of Howard-Busse. *Physica D* **121** (1), 175 – 192.

Kessar, M., Plunian, F., Stepanov, R. & Balarac, G. 2015 Non-Kolmogorov cascade of helicity-driven turbulence. *Phys. Rev. E* **92**, 031004(R).

Kraichnan, R. 1973 Helical turbulence and absolute equilibrium. *J. Fluid Mech.* **59**, 745–752.

Ladyshenskaya, O. A. 1969 *The Mathematical Theory of Viscous Incompressible Flow.*, 2nd edn. Gordon and Breach, New York.

Landau, L. D. & Lifshitz, E. M. 1959 *Fluid Mechanics*, English edn. Pergamon Press, London.

Leray, J. 1934 Sur le mouvement d'un liquide visqueux emplissant l'espace. *Acta Mathematica* **63**, 193–248.

Li, Y., Meneveau, C., Chen, S. & Eyink, G. L. 2006 Subgrid-scale modeling of helicity and energy dissipation in helical turbulence. *Phys. Rev. E.* **74**, 026310.

Lilly, D. K. 1967 The representation of small scale turbulence in numerical simulation experiments. In *Proc. IBM Scientific Computing Symposium on environmental sciences* (ed. H. H. Goldstine), pp. 195–210. International Business Machines Corporation (IBM). Data Processing Division.

Lilly, D. K. 1986 The structure, energetics, and propagation of rotating convective storms. Part II: Helicity and storm stabilization. *J. Atmos. Sci.* **43**, 126–140.

Lumley, J. L. 1992 Some comments on turbulence. *Phys. Fluids A* **4**, 203–211.

McComb, W. D., Berera, A., Salewski, M. & Yoffe, S. R. 2010 Taylor's (1935) dissipation surrogate reinterpreted. *Phys. Fluids* **22**, 61704.

McComb, W. D., Berera, A., Yoffe, S. R. & Linkmann, M. F. 2015 Energy transfer and dissipation in forced isotropic turbulence. *Phys. Rev. E* **91**, 043013.

Mininni, P. D. & Pouquet, A. G. 2010*a* Rotating helical turbulence. I. Global evolution and spectral behavior. *Phys. Fluids* **22**, 035105.

Mininni, P. D. & Pouquet, A. G. 2010*b* Rotating helical turbulence. II. Intermittency, scale invariance, and structures. *Phys. Fluids* **22**, 035106.

Moffatt, H. K. 1969 The degree of knottedness of tangled vortex lines. *J. Fluid Mech.* **35**, 117–129.

Moffatt, H. K. 1985 Magnetostatic equilibria and analogous Euler flows of arbitrarily complex topology. Part 1. Fundamentals. *J. Fluid Mech.* **159**, 359378.

Moffatt, H. K. 2014 Helicity and singular structures in fluid dynamics. *Proc. Natl. Acad. Sci.* **111** (10), 3663–3670.

Nicodemus, R., Grossmann, S. & Holthaus, M. 1998 The background flow method. part 1. constructive approach to bounds on energy dissipation. *J. Fluid Mech.* **363**, 281300.

Polifke, W. & Shtilman, L. 1989 The dynamics of helical decaying turbulence. *Phys. Fluids A* **1**, 2025–2033.

Rollin, B., Dubief, Y. & Doering, C. R. 2011 Variations on Kolmogorov flow: turbulent energy dissipation and mean flow profiles. *J. Fluid Mech.* **670**, 204–213.

Sahoo, G. & Biferale, L. 2015 Disentangling the triadic interactions in Navier-Stokes equations. *Eur. Phys. J. E* **38**, 1–8.

Smagorinsky, J. 1963 General circulation experiments with the primitive equations. *Mon. weath. Rev.* **91**, 99–164.

Sreenivasan, K. R. 1984 On the scaling of the turbulence dissipation rate. *Phys. Fluids* **27**, 1048–1051.

Sreenivasan, K. R. 1995 On the universality of the Kolmogorov constant. *Phys. Fluids* **7**, 2778–2033.

Sreenivasan, K. R. 1998 An update on the energy dissipation rate in isotropic turbulence. *Phys. Fluids* **10**, 528.

Stepanov, R., Golbraikh, E., Frick, P. & Shestakov, A. 2015 Hindered energy cascade in highly helical isotropic turbulence. *Phys. Rev. Lett.* **115**, 234501.

Tannehill, J. C., Anderson, D. A. & Pletcher, R. A. 1997 *Computational Fluid Mechanics and Heat Transfer*, 2nd edn. Taylor and Francis, Washington, D.C.

Valente, P. C., Onishi, R. & da Silva, C. B. 2014 Origin of the imbalance between energy cascade and dissipation in turbulence. *Phys. Rev. E* **90**, 023003.

Valente, P. C. & Vassilicos, J. C. 2012 Universal dissipation scaling for nonequilibrium turbulence. *Phys. Rev. Lett.* **108**, 214503.

Vassilicos, J. C. 2015 Dissipation in Turbulent Flows. *Annu. Rev. Fluid Mech.* **47**, 95–114.

Waleffe, F. 1992 The nature of triad interactions in homogeneous turbulence. *Phys. Fluids A* **4**, 350–363.

Wang, L.-P., Chen, S., Brasseur, J. G. & Wyngaard, J. C. 1996 Examination of hypotheses in the Kolmogorov refined turbulence theory through high-resolution simulations. Part 1. Velocity field. *J. Fluid Mech.* **309**, 113–156.

Yeung, P. K., Donzis, D. A. & Sreenivasan, K. R. 2012 Dissipation, enstrophy and pressure statistics in turbulence simulations at high Reynolds numbers. *J. Fluid Mech.* **700**, 5–15.

Yeung, P. K., Zhai, X. M. & Sreenivasan, K. R. 2015 Extreme events in computational turbulence. *PNAS* **112**, 1263312638.

Yokoi, N. & Yoshizawa, A. 1993 Statistical analysis of the effects of helicity in inhomogeneous turbulence. *Phys. Fluids A* **5**, 464–477.